EGTRIB Journal
JOURNAL OF
THE EGYPTIAN SOCIETY OF TRIBOLOGY
VOLUME 20, No. 4, October 2023, pp. 27 – 43 **ISSN 2090 - 5882**
(Received June 29. 2023, Accepted in final form August 22. 2023) **jest.journals.ekb.eg**

TRIBOLOGY DIGITAL TWIN OF AIRCRAFT CARBON-CARBON COMPOSITE DISC BRAKES

Amro M. Youssef[1], Eslam M. Hussein[2], Tarek M. El Wasif[3] and Ahmed Esmat Hussien[3]

[1]High Institute for engineering and technology Alobour,
[2]Egyptian Ministry of Defense,
[3]Arab Academy for Science and Technology and Maritime Transport.

ABSTRACT

Friction and wear are two major factors that affect the service life of disc brakes. Carbon-carbon (C/C) composite materials have superior and stable friction properties, which make them suitable for use as friction materials in aircraft and high-performance brakes. This article presents a wear simulation method for predicting wear out amount of C/C brake discs under specified operating conditions. An updated version of Archard's wear equation is used in the contact domain to predict the wear progression of the friction surfaces. COMSOL Multiphysics®5.5 is used to simulate wear by solving the governing differential equations. Frictional heat generation is simulated by considering the effects of heat on the material's thermal properties and resulting surface deformation. Element removal technique is used to simulate the change in disc thickness due to material loss. The wear progression with time is presented, and the wear model is verified using experimental work from the literature.

KEYWORDS

Digital twin, mission engineering, tribology, wear, friction, finite element, carbon-carbon composite.

INTRODUCTION

Product service life is often limited by the loss of material from its surfaces, this process is defined as wear, [1]. Wear occurs when two surfaces rub against each other, causing frictional heat generation, deformation, and the presence of contaminants and wear debris. These factors make it difficult to accurately model wear criteria, [2, 3]. However, significant research has been conducted to develop wear models that can

describe different wear modes [4] able to forecast wear rate of materials and components and to design products that are more resistant to wear.
Archard's predictive equation has been widely used and cited in many scientific research papers, [1, 8 - 10], as the first model to use dimensional analysis to describe the phenomenon, [5, 6]. The model depends on several parameters, such as the applied pressure on contact surfaces, sliding areas, and material hardness, [7]. However, there is no single predictive wear equation that can be universally applied to all cases, [11, 12]. Therefore, many researchers have used finite element simulation to study the sliding wear under different conditions. For example, Molinari et al, [13], used a finite element model based on a modified Archard's wear equation to study the dry sliding wear. Other studies, [14 - 16] have also simulated the wear behavior of various materials using different models.

Carbon/Carbon disc brakes use carbon fiber reinforced carbon matrix composites as friction material. They are widely used in military aircraft because it is lighter and stronger, with higher thermal conductivity and lower thermal expansion, better friction and wear properties, and lower oxidation and corrosion rates, which make them more durable and resistant to harsh environmental conditions.

Tribological behavior of Carbon/Carbon composite studies investigating several parameters such as applied load, [8], sliding speed, [17], sliding distance, [18], fiber orientation, fiber type, fiber size and length [19], heat treatment process [20] and construction of the disc brake, [21]. Carbon/Carbon composite disc brakes are used in both hypercars, jet fighters and commercial aircrafts, [17, 18, 22-24].

This research project demonstrates how mission engineering and digital twins can work together to develop an aircraft braking system while adopting wear problem with a mission engineering in focus. The digital twin was built using COMSOL Multiphysics® to integrate relevant wear models and multiphysics simulations with braking strategy, airplane configuration, the environment, the mission objectives, and the adversaries to represent the physics relation to safety, lifetime, and speed.

Using COMSOL Multiphysics software the finite element wear model is a result of the interaction of five modules, 1) tabulated mission parameters, 2) multi-body dynamics to simulate the contact pressure between the stator and rotor discs, 3) Wear rate calculation, 4) Heat transfer due to friction, 5) Solid mechanics to simulate the mechanical stresses in the disc during braking. After each solution time step, the model updates braking disc thicknesses after weight loss due to wear.

WEAR MODEL SIMULATION

Wear Modified Equation

Archard's wear law relates the object thickness change rate (material loss) to wear coefficient, k, sliding velocity, $v(t)$, and contact pressure, $p(t)$, [1, 5, 17, 19]. The height variation of the discs is an indication of material wear and is expressed in the simulation problem as:

$$\frac{\Delta h}{\Delta t} = k\, p(t)\, v(t) \qquad (1)$$

Wear Modeling Procedure

The tribology digital twin process is carried out as shown in Fig. 1. The procedure starts by simulating the physics of contact mechanics of the finite element model which includes modelling the brake discs geometry in contact, utilizing material properties and applying boundary conditions. The status of each node on the sliding surface is determined by the solution of the contact problem, which updates with each time step according to the contact pressure at each surface.

Modified Archard's Wear Equation is used to simulate the wear process as an ordinary differential equation, inside the model where the sliding velocity of every local element is known and consequently the reduction in thickness of the discs can be calculated. The shape of the contact surface changes over time due to progressive boundary updates due to material removal. However, with the applied pressure and the incremental wear, the contact surface is averaged to smooth the curve for the upcoming iteration. The depth of discs wear frictional contact surfaces is calculated as the median of local value of vertical boundary displacement at every surface node. When a certain film of the material is removed, presented as thickness reduction, because of wear modeling the model starts to update the geometry with the new height and calculate the distribution for the contact pressure. Elements of the surface film of each contact surface are removed from the finite element model according to the amount of material loss at this wear iteration. The new geometry mesh is regenerated to calculate and simulate the contact pressure and wear process. This operation is done in a closed loop till the end of the braking process, [2, 21, 25].

The mission parameters as well as the heat transfer solution are integrated into the simulation model to calculate the heat generated during braking and the temperature distribution, respectively. The heat affects the wear rate of the discs by causing thermal stresses, reducing the friction coefficient between the stator and the rotor, which can decrease the braking efficiency and increase the wear rate. The last parameter is the rise in temperatures that tends to oxidize and corrode the disc surface, which can degrade the disc quality and increase the wear rate.

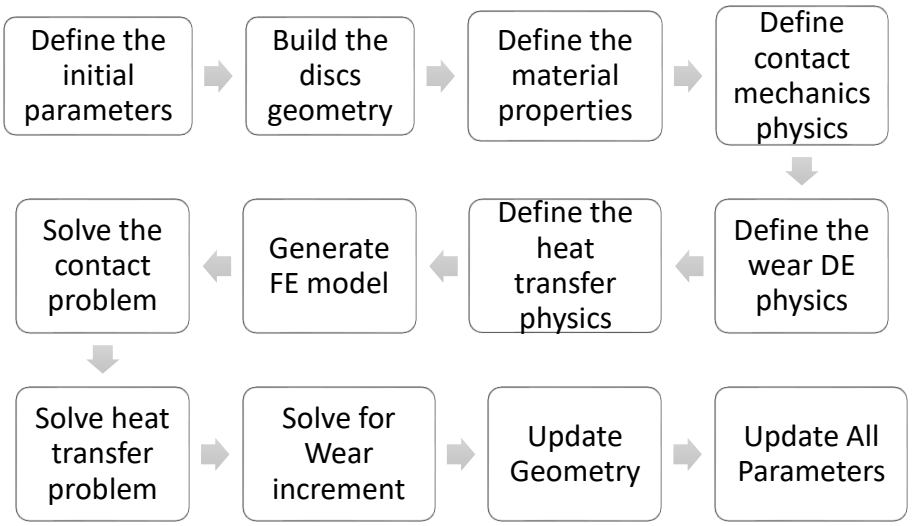

Fig. 1 Aircraft brake digital twin chart.

AIRCRAFT BRAKE DIGITAL TWIN

Aircraft brake system consists of stationary discs fixed to the landing gear and rotating discs that are attached to the wheels as shown in Fig. 2. When the brakes are applied, hydraulic/mechanical or pneumatic pressure pushes the discs together, creating friction and normal force that generates the torque needed to reduce the aircraft velocity.

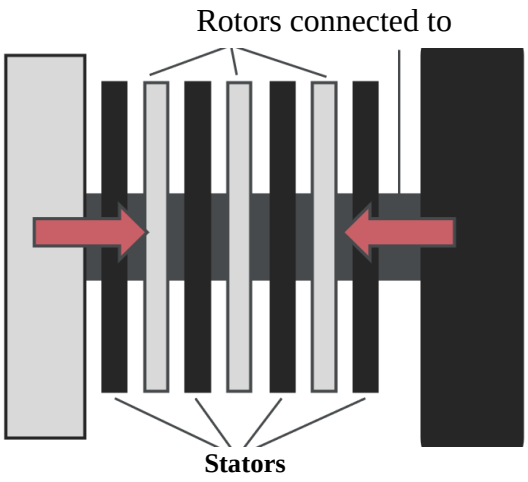

Fig. 2 Aircraft brake assembly.

Disc Brake Model Geometry, and Assumptions.

In this case, the aircraft brakes consist of seven discs, as shown in Fig. 3. Three rotating discs are surrounded by four stationary discs. The actuating system applies an axial force to the disc set. This model is simulated as a 2D axisymmetric problem without sacrificing accuracy. The braking pressure is equivalently distributed on the pressure plate surface. Fixed boundary conditions are used in the back pressure plate.

The wheel hub, oil piston master, housing and wheel spindle are neglected in the simulation model. The Carbon/Carbon composite disc brake material is assumed to be quasi-isotropic in mechanical and thermal properties. Each film removed by wear has a uniform small thickness compared to the thickness of the disc laminates. Also, the disc thickness variation due to temperature is neglected due to the intermittent nature of the braking process and the low thermal expansion coefficient of the material.

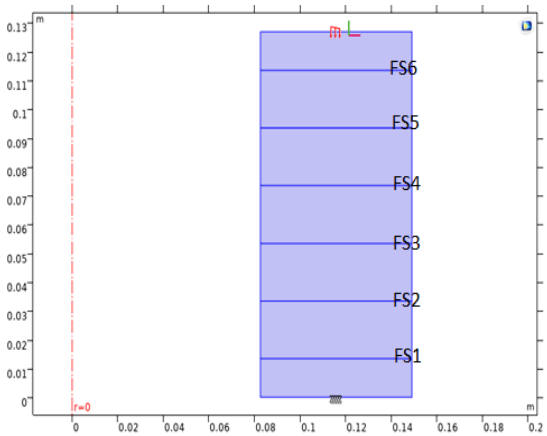

Fig. 3 2D Axi-symmetric aircraft brake model of friction surfaces.

All the discs are made from the same material with the same manufacturing process. Both the stator and the rotor discs have the same dimension also the back plate and the end plate have the same dimension, as these two discs need only a single friction surface are shown in Table 1. Carbon-carbon composite isotropic material properties, [25] are shown in Table 2.

Table 1. Disc brake dimensions

Disc type	Inner diameter (mm)	Outer diameter (mm)	Thickness (mm)
Stator and rotor discs	82.5	149	20
Backplate and end plate	82.5	149	13

Finite Element Model

A 2D axisymmetric model is built using COMSOL Multiphysics® to solve wear of carbon/carbon composite brake discs wear, where the friction contact surfaces are the heat sources, and the material loss surfaces during braking. Solid mechanics physics is used to define the pressure applied by the braking system to the pressure plate and the fixed constraint on the boundary of the back plate. Six contact pairs are defined for six friction surfaces, as shown in Fig. 3: FS1, FS2, FS3, FS4, FS5 and FS6.

Table 2. Carbon-Carbon composite material properties

Properties	Units	Disc
Material Density	kg/m^3	1800
Laminate Longitudinal Young's Modulus, E_x	GPa	50.9
Laminate Transverse Young's Modulus, E_z	GPa	5.89
Poisons ratio, $\upsilon_{r\Theta}$		0.3
Transverse Poisons ratio, υ_{rz}		0.33
Modulus of Rigidity, G_{rz}	GPa	2.46
Radial coeff. Of Thermal conductivity, k_r	W/mK	50
Transverse coeff. Of Thermal conductivity, k_z	W/mK	10
Specific Heat, C_p	J/kg.K	1420
Radial Thermal expansion, α_r (10^{-6}/K)		0.31
Transverse Thermal expansion, α_z (10^{-6}/K)		0.29

A modified version of Archard's Wear Equation is used to detect material losses by solving it for each friction surface. The result gives an indication of the depth of wear for every element. Refined mesh was used on the surface to enhance the results as shown in Fig. 3.

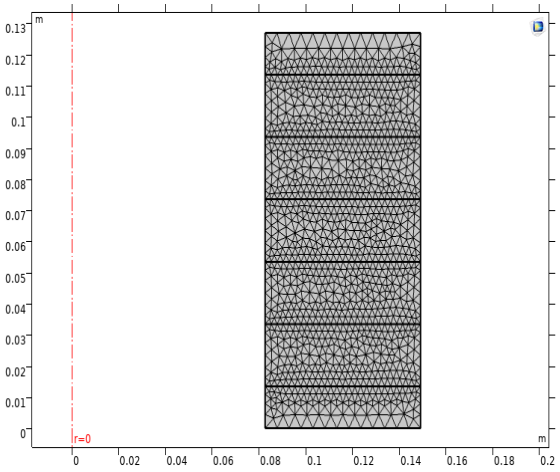

Fig. 4 2D Axisymmetric brake system mesh build.

Mission Parameters, Braking Torque and Heat Dissipation

In any mechanical system, the heat dissipated to stop or slow down the vehicle is equivalent to the energy extracted from the system. The mechanical equivalent of heat is equal to the change in kinetic energy during braking interval and also the work added to the system if presented.

In the case of stopping aircraft, the total energy can be calculated as:

$$E = \frac{1}{2} N I \omega^2 + \frac{1}{2} m v^2 + Wa \qquad (2)$$

$$W = \Delta E = \Delta KE + Wa \qquad (3)$$

Where E is the total energy, ω is the angular velocity, m is the total aircraft mass , I is the wheel mass moment of inertia, N the number of wheels, W is the total work for stopping the vehicle, Wa represents the work added to the system whatever it is positive or negative work [26].

The kinetic energy generated by wheel brake discs' rotary movement is frequently insignificant in comparison to the kinetic energy generated by translation [26] thus, the brake retardation power is evaluated by the first derivative of the vehicle kinetic energy:

$$\mathbf{P = -m\, v(t)\, a(t)} \qquad \mathbf{(4)}$$

Where, m, is the total aircraft mass, v(t) is the aircraft speed, and a(t) is the deceleration.
The heat power per unit area is obtained from the following equation:

$$\mathbf{q = \mu(t)\, P\, v(t)} \qquad \mathbf{(5)}$$

Where, q, is the heat power of friction surfaces per unit area, P is the specific pressure between brake discs, $\mathbf{v(t)}$ is the aircraft speed and $\boldsymbol{\mu}(\mathbf{t})$ is the friction coefficient during braking.

Heat flow between discs is governed by the heat equation which describes the heat flow between discs as shown:

$$\rho\, C_p \frac{\partial T}{\partial t} + \nabla(-k\nabla T) = \rho\, C_p\, v\Delta T \qquad \mathbf{(6)}$$

Where C_p is the heat capacity of the disc material, ρ the density of the disc material, k is the thermal conductivity of the disc material and v is the local velocity vector of the discs [2, 3, 27]. During aircraft braking, the air is forced toward the brake discs with a velocity assumed to be the same as the aircraft velocity. This acts as forced convection which works on dissipating the heat energy due to braking. To account for heat dissipated to the ambient environment, heat transfer by forced convection is defined on all boundaries and is calculated as:

$$\mathbf{q = h\,(T_{ex} - T)} \qquad \mathbf{(7)}$$

Where q is heat flux across the surface due to forced convection, h, is the convection heat transfer coefficient, T_{ex}, is external surface temperature and T is the ambient temperature [2, 3, 27]. Heat is dissipated to the surrounding by radiation and is taken into consideration for all the discs' boundaries as

$$q = \varepsilon \sigma (T_{sur}^4 - T^4) \qquad (8)$$

Where, ε , is the emissivity, σ is the Boltzmann constant, T_{sur} and T are the temperatures of the discs and surrounding [2, 3, 27]. Work done to stop the aircraft is converted into heat between the friction surfaces. The braking torque required to slow down the aircraft at constant deceleration is related to the total work done in stopping the aircraft

$$W = \frac{(\omega_o + \omega_f)}{2} T t \qquad (9)$$

Where, T braking torque, ω_o is the initial angular velocity, ω_f is the final angular velocity and t is the braking time. The braking pressure is the main cause of the braking torque as the pressure plate compresses the discs with certain pressure resulting in braking torque and this torque can be calculated as:

$$T = \frac{2n}{3\sqrt{3}} \mu P r_o^3 \qquad (10)$$

Where, n is number of contact surfaces, μ is the disc friction coefficient, P is the contact pressure and r_o is the outer radius of the brake disc, [26].

Practical Case Study

An F-16 aircraft landing guidelines will be simulated. Table 3 presents the aircraft mass, landing speed, deceleration rate, environmental temperature, braking time, braking pressure calculated from the braking torque and energy change to stop the aircraft.

The landing weight of a military aircraft determines its landing velocity, which in turn affects the braking strategy. This study defines two membership functions for velocity and deceleration, and explicitly defines the braking pressure based on these functions. The results are shown in Fig. 5 and Fig. 6.

Table 3. Aircraft braking conditions

Material property		disc	Units
Aircraft Mass	m_{plan}	9000	Kg
Wheel Radius	r_{wheel}	0.352	M
Initial Aircraft Touch-Down Speed	v_0	260	km/hr
Initial Vehicle Acceleration	a_0	3.611	m/s^2
Air Temperature	T_{air}	300	^oK
Braking Time (Start)	t_{start}	1	S
Braking Time (End)	t_{end}	21	S
Wear Coefficient	K	7×10-14	Pa^{-1}
Braking Pressure	P	0.`7	MPa

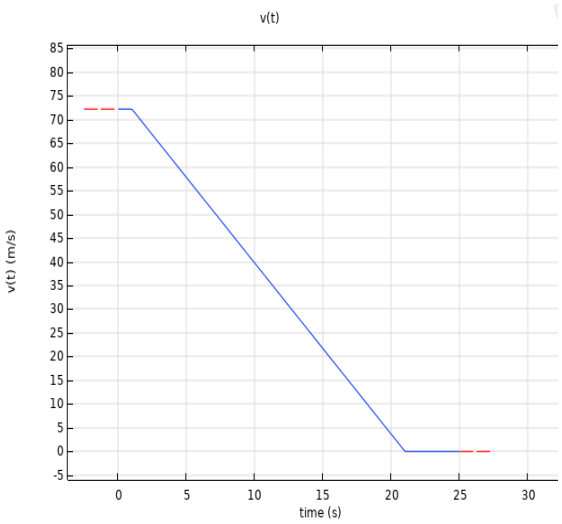

Fig. 5 Aircraft braking velocity.

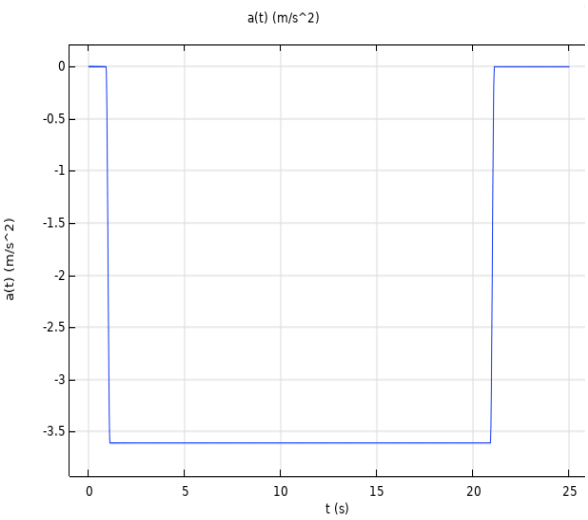

Fig. 6 Aircraft braking deceleration.

Wear coefficient measurement

The experimental test, according to ASTM D3702, is to determine the friction coefficient and wear rate of self-lubricated materials in rubbing contact. The test was performed using a universal thrust washer testing machine, which applies a normal load to a rotating specimen. The wear rate is determined by measuring the change in thickness of the specimen over time, and the coefficient of friction is determined by measuring the torque required to rotate the specimen.

The test machine rotates a test specimen against a stationary steel washer under a load. Each test begins with a 40-hour break-in period, followed by a selected test duration. Both the break-in period and the test duration are conducted at the same normal load and speed. The load is applied by dead weights on a 10:1 lever arm. The

contact area is 1.8 cm^2. The mean rubbing velocity is calculated based on the spindle rotational speed. For example, a spindle rotational speed of 1000 rpm is equivalent to a mean rubbing velocity of 1.6 m/min.

The geometries (in mm) of the rotor and stator test specimens are shown in Error! R eference source not found. **(a) and** Error! Reference source not found. **(b). The holes (1 and 2) in** Error! Reference source not found. **(b) show the fixations holes for both the r otor and the stator test specimens.**

Experiments were performed at room temperature with relative humidity of 45 % to 55 %, using the following testing parameters: an applied load of 0.7 MPa, a rotating speed of 1910 rpm, and a testing time of 12 minutes.

A thermocouple installed within 2 mm under the friction contact surface of the stator test specimen was used to measure the temperature, as shown in Error! Reference s ource not found.**. Friction torque was also measured during the experiment, and the coefficient of friction was obtained from these measurements. The weight loss was measured using a weighting balance of 10^{-4} grams resolution. The experiment was repeated three times, and the weight loss was measured three times and averaged for each experiment.**

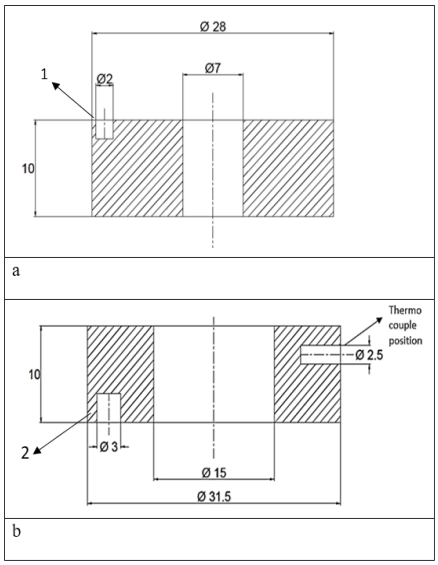

Fig. 7 Geometry of (a) Static specimen, (b) Rotating specimen.

The average of the coefficient of friction is found to be $24.3x10^{-2}$ and the wear coefficient is detected depending on Archard's wear equation and is found to be 7e-

14. Many researchers represented the friction coefficient value as a constant value, [2, 3, 25, 29]. The friction coefficient was represented in the simulation as a tabulated temperature-dependent function reflecting the measured friction coefficient values presented in Fig. 8 as a function of temperature.

During testing, as shown in Fig. 8, Carbon/Carbon composite materials had transitional change at temperature of 150ºC where the friction coefficient increases abruptly from 0.1 to 0.6 and then decreases to 0.25. This transition occurred when the removed abrasive particles start to affect both friction surfaces. By increasing heat and under the applied pressure, these abrasive particles will form a fine lubricant layer of powder reducing the friction coefficient which will act as lubricant between both surfaces. This phenomenon gives the C/C composite material the advantage of self-lubricating to reduce the material loss due to friction and these results were matched with Blanco, [19].

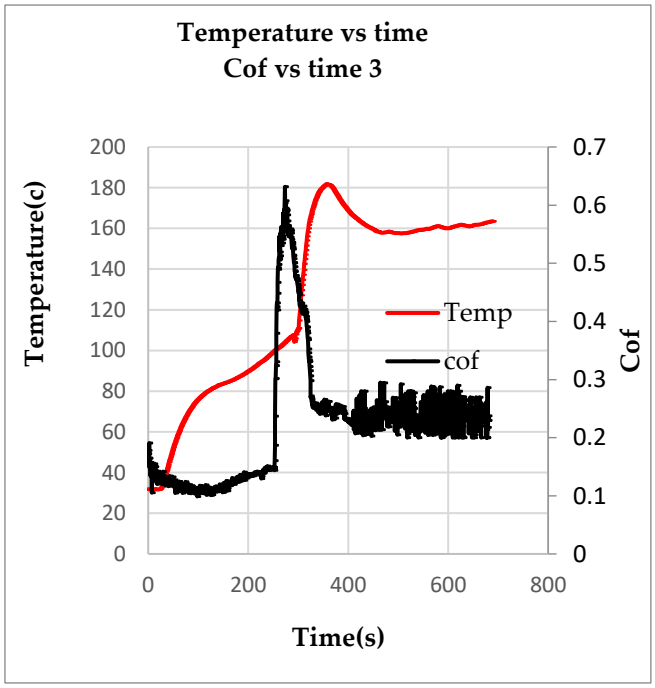

Fig. 8 Temperature, coefficient of friction vs time.

Wear model validation

Wear model validation test specimens is tested at two speeds, 1400 rpm and 2000 rpm. A braking pressure of 1.7 MPa is applied. The results showed that the time required to stop a rotor specimen with speeds 1400 rpm and 2000 rpm were 26 sec and 40 sec, respectively. The coefficient of wear is calculated using Archard's wear equation, as the weight loss can be calculated by weighing the test specimens before and after the test [8, 28].

$$k = \frac{\Delta V}{F\, v\, t} \qquad (11)$$

Where, ΔV is the wear volume, F applied load, v, sliding velocity, and t is time. Similar results were obtained by Zhao [2] for weight loss and wear coefficient. Similar measurements are shown in Table 4 for the weight loss validated with Lee et al, [23], work. The value of the wear coefficient of 4.69E-14 Pa^{-1} obtained experimentally is used in the COMSOL Multiphysics model as a parameter in Archard's Wear differential equation solver to predict the amount of wear for aircraft brakes.

Table 4. Weight Loss and Wear Coefficient Measurements

	Weight Loss (mg)		Wear Coefficient Pa^{-1}	
Sliding Speed (rpm)	**1400**	**2000**	**1400**	**2000**
Lee et al [23]	**1**	**2**		
Zhao [2]	**0.985**	**1.972**	**4.73E-14**	**4.3E-14**
Current Study	**1.05**	**2**	**4.69E-14**	**3.82E-14**

RESULTS AND DISCUSSION

The model was designed to simulate the actual braking process. When brake pressure is applied, it causes friction and heat production, which leads to material loss. The contact pressure between the friction surfaces is not constant throughout the braking process, even though the braking pressure applied to the discs is constant. The contact pressure between the friction surfaces is non-uniformly distributed across the contact area, with the highest pressure at the center of the friction surfaces and decreasing towards the edges of the discs. This is illustrated in Fig. 9.

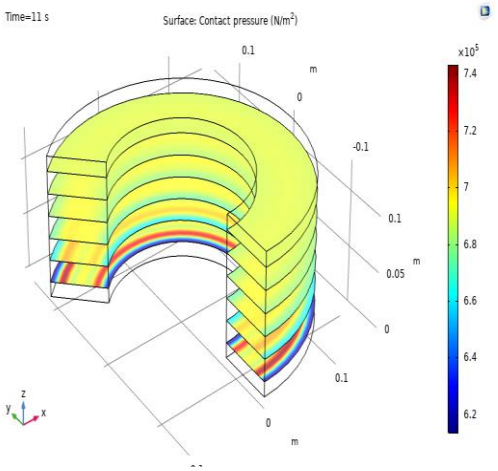

Fig. 9 Pressure distribution between contacting surfaces at t = 11sec.

Fig. 10 **shows the contact pressure over the disc radius for friction surface number 6 (FS6) during the braking operation where the pressure distribution changes with time for the single friction surface. The pressure value progresses from the center to the end of the disc, these changes affect material loss and surface morphology. That is referenced by the radial variation of contact pressure.**

By representing pressure distribution for friction surface at different times as shown in Fig. 12 it can deduced that pressure distribution is changing during braking for all friction surfaces. Irregular decreases in contact pressure are perceived at the inner and outer radii, which indicate a loss of contact or diminished contact. These changes are due to the temperature effect on the disc brake material where the discs' temperature increase due to heat generation and friction between the discs. This increase in temperature also affects the material properties.

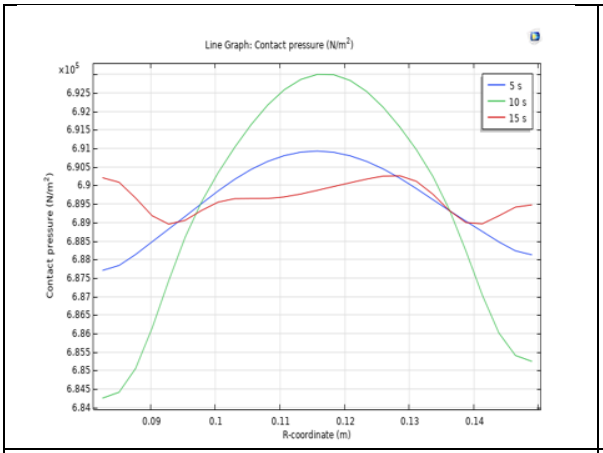

Fig. 10 Friction surface #6 Contact pressure vs. disc radius at different test time instances.

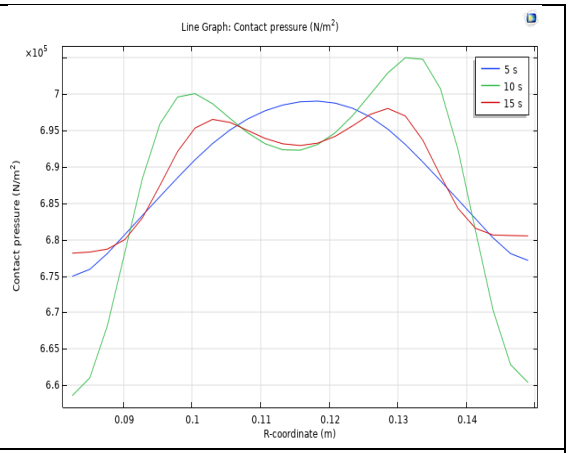

Fig. 11 Friction surface #2 Contact pressure vs. disc radius at different test time instances.

The outer discs with friction surfaces 1, 2, 5 and 6 exhibit less temperature rise due to healthier heat dissipation to the surrounding. The middle rotor disc with friction surfaces 3 and 4 exhibit higher temperature rise, which affects the thermal deformation, contact pressure and the wear rate on those discs. The discs' temperature distribution at t = 21 sec. is higher rotor disc mid-point at the friction surfaces 3 and 4, while it has a lower value at the pressure plate and end plate as shown in Fig. 12.

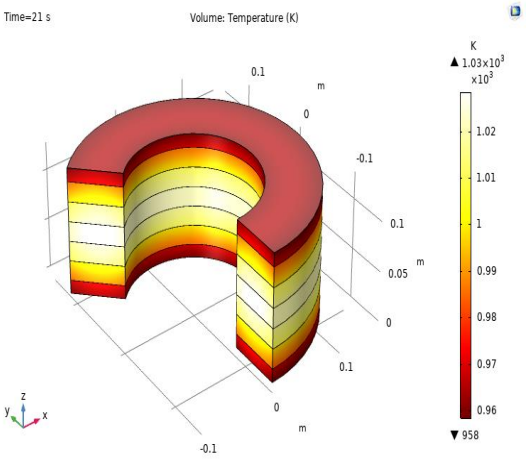

Fig. 12 Disc temperature distribution at end of braking process.

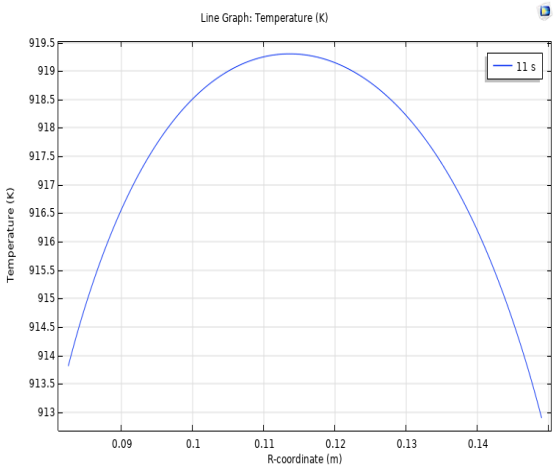

Fig. 13 Temperature vs. disc radius for Friction surface #3 at t = 11sec.

Also, the non-uniform temperature distribution on the disc surfaces as shown in Fig. 13 can be attributed to the non-uniform contact pressure on discs. That will have a great effect on the discs deformations and consequently the wear. The lower temperatures of the inner and outer radii (disc ends) of the annular discs in comparison to the interior friction surfaces at the middle of the disc. This may be attributed to heat dissipation. The outer surfaces of the discs show lower temperatures due to better heat dissipation to the system surroundings by thermal convection and radiation.

Wear depth is illustrated in Fig. 14 for the contact surfaces at t = 21 sec during the braking process of the aircraft. It can be seen that the wear depth is not uniform, this may be attributed to the non-uniform contact pressure and the variation of sliding velocity along the disc radius. It can be inferred that the wear depth increases when moving from the inner radius to the outer radius as the sliding speed increases near to the outer radius. At the end of the braking process, the largest value of wear is 14.7 μm. This is consistent with Archard's wear equation, as the contact pressure and the sliding speed, affect the friction surface wear amount.

Fig. 15 shows the wear depth of selected elements on friction disc #1 along the radius of the disc brake. The wear depth is not uniform across the disc friction surface. An average value of the nodal wear is calculated and used in the element removal technique for future iterations.

The wear depth of material during the whole braking process for friction disc#1 in one-second increments is presented in Fig. 16. It showed that, the wear depth

increases with time, where the value increases along the disc radius from inside out. This may be attributed to the increase of the sliding toward the edge. The wear depth slope is decreasing because the sliding velocity is decreasing with time (braking process). Frictional heat generation and wear amount will also decrease as the sliding speed is decreasing as explained by the reduction of aircraft speed.

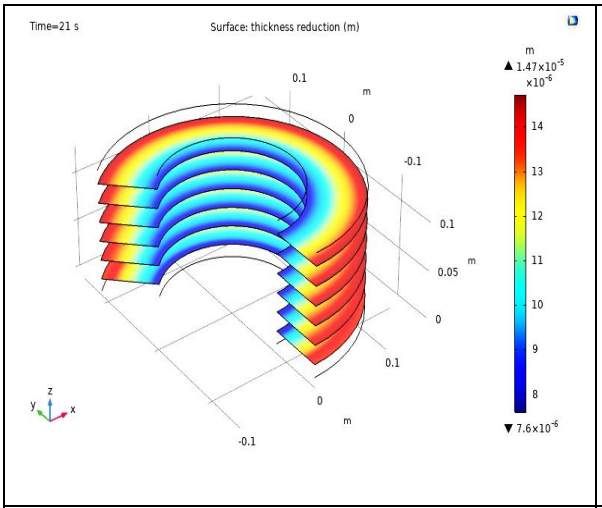

Fig. 14 Wear depth for contact surfaces at t = 21 sec.

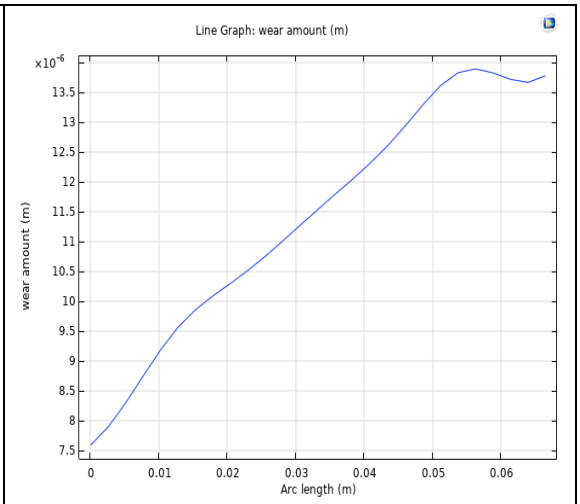

Fig. 15 Friction surface #1 wear progression vs. disc radius at t = 20 sec.

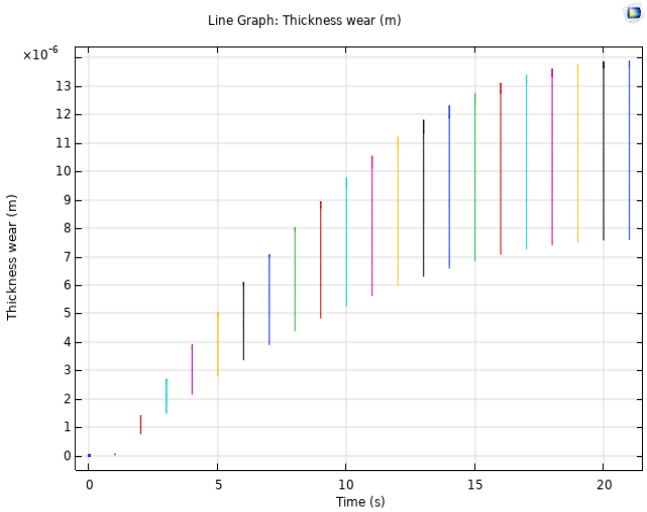

Fig. 16 FS1 wear depth variation vs time during braking operation.

CONCLUSIONS

The braking problem simulation models frictional heat generation and heat dissipation by forced convection and radiation. This affects the friction coefficient, contact pressure, and wear amount. Material removal is used to update the surface geometry and remeshing. Material wear rate graphs show that wear increases near

the disc outer radius as sliding speed increases. This can be used to anticipate braking disc lifetime based on braking strategy and environment. A mission engineered digital twin of the wear phenomena of Carbon/Carbon composite multidisc aircraft brake was built and validated based on a modified version of Archard's Wear Equation.

REFERENCES

1. Archard J., and Hirst W., "The wear of metals under unlubricated conditions," in Proceedings of the Royal Society of London A: Mathematical, Physical and Engineering Sciences, 1956, vol. 236, no. 1206: The Royal Society, p. 397, B. Bhushan, Principles and applications of tribology. John Wiley & Sons, (2013).

2. Zhao S., Hilmas G. E., and Dharani L. R., "Numerical simulation of wear in a C/C 988", (1953).

3.composite multidisc clutch," Carbon, vol. 47, no. 9, pp. 2219-2225, (2009).

4. Zhao S., Hilmas G. E., and Dharani L. R., "Behavior of a composite multidisc clutch subjected to mechanical and frictionally excited thermal load," Wear, vol. 264, no. 11-12, pp. 1059-1068, (2008).

5. Meng H., and Ludema K., "Wear models and predictive equations: their form and content," Wear, vol. 181, pp. 443-457, (1995).

6. Archard J., "Contact and rubbing of flat surfaces," Journal of applied physics, vol. 24, no. 8, pp. 981--410, (1981).

7. Montgomery S., Kennedy D., and O'Dowd N., "Analysis of wear models for advanced coated materials," (2009).

8. Gomes J., Silva O., Silva C., Pardini L., and Silva R., "The effect of sliding speed and temperature on the tribological behaviour of carbon–carbon composites," Wear, vol. 249, no. 3, pp. 240-245, (2001).

9. Söderberg A., and Andersson S., "Simulation of wear and contact pressure distribution at the pad-to-rotor interface in a disc brake using general purpose finite element analysis software," Wear, vol. 267, no. 12, pp. 2243-2251, (2009).

10. Friedrich K., Reinicke R., and Zhang Z., "Wear of polymer composites," Proceedings of the Institution of Mechanical Engineers, Part J: Journal of Engineering Tribology, vol. 216, no. 6, pp. 415-426, (2002).

11. Hsu S., Shen M., and Ruff A., "Wear prediction for metals," Tribology International, vol. 30, no. 5, pp. 377-383, (1997).

12. Williams J. a. A., "Wear modelling: analytical, computational and mapping: a continuum mechanics approach," Wear, vol. 225, pp. 1-17, (1999).

13. Molinari J., Ortiz M., Radovitzky R., and Repetto E., "Finite-element modeling of dry sliding wear in metals," Engineering Computations, vol. 18, no. 3/4, pp. 592-610, (2001).

14. Gonzalez C. et al., "Numerical analysis of pin on disc tests on Al–Li/SiC composites," Wear, vol. 259, no. 1-6, pp. 609-612, (2005).

15. Kim N. H. et al., "Finite element analysis and experiments of metal/metal wear in oscillatory contacts," Wear, vol. 258, no. 11-12, pp. 1787-1793, (2005).
16. Hegadekatte V., Huber N., and Kraft O., "Finite element based simulation of dry sliding wear," Modelling and Simulation in Materials Science and Engineering, vol. 13, no. 1, p. 57, (2004).
17. Chen J., and Ju C., "Effect of sliding speed on the tribological behavior of a PAN-pitch carbon-carbon composite," Materials chemistry and physics, vol. 39, no. 3, pp. 174-179, (1995).
18. Chen J., Lin J. C., and Ju C., "Effect of load on tribological behaviour of carbon-carbon composites," Journal of materials science, vol. 31, no. 5, pp. 1221-1229, (1996).
19. Blanco C., Bermejo J. Marsh H., and Menendez R., "Chemical and physical properties of carbon as related to brake performance," Wear, vol. 213, no. 1-2, pp. 1-12, (1997).
20. Rao J., Sinnur K., and Jain R., "Effect of weave texture of carbon fabric on mechanical, thermal and tribological properties of carbon/carbon aircraft brakes," Int. J. Compos. Mater, vol. 5, pp. 89-96, (2015).
21. Luo R., Huai X., Qu J., Ding H., and Xu S., "Effect of heat treatment on the tribological behavior of 2D carbon/carbon composites," Carbon, vol. 41, no. 14, pp. 2693-2701, (2003).
22. Buckley J. D., and Edie D. D., Carbon-carbon materials and composites. William Andrew, (1993).
23. Lee K., Lin J. C., and Ju C.-P., "Surface effect on braking behavior of PAN-pitch carbon-carbon composite," Wear, vol. 199, no. 2, pp. 228-236, (1996).
24. Yen B., "An investigation of friction and wear mechanisms of carbon-carbon composites in nitrogen and air at elevated temperatures," Carbon, vol. 34, no. 4, pp. 489-498, (1996).
25. Choi J.-H., Han J.-H., and Lee I., "Transient analysis of thermoelastic contact behaviors in composite multidisc brakes," Journal of Thermal Stresses, vol. 27, no. 12, pp. 1149-1167, (2004).
26. Orthwein W. C., Clutches and brakes: design and selection. CRC Press, (2004).
27. Zhang C., Zhang L., Zeng Q., Fan S., and Cheng L., "Simulated three-dimensional transient temperature field during aircraft braking for C/SiC composite brake disc," Materials & Design, vol. 32, no. 5, pp. 2590-2595, (2011).
28. Podra P., and Andersson S., "Simulating sliding wear with finite element method," Tribology international, vol. 32, no. 2, pp. 71-81, (1999).